Journal of the Physical Society of Japan **86**, 044401 (2017)
https://doi.org/10.7566/JPSJ.86.044401

First-Principles Assisted Prediction of the Nonlinear Optical Behavior of $Mg_3B_7O_{13}Cl$ Crystal

Yanzhou Sun[1], Zhi Li[2], Ming-Hsien Lee[2,3]*, Zhihua Yang[2], Shilie Pan[2], and Beysen Sadeh[1]*

[1]*School of Physics Science and Technology, Xinjiang University, Urumqi 830046, China*
[2]*Key Laboratory of Functional Materials and Devices for Special Environments of CAS, Xinjiang Key Laboratory of Electronic Information Materials and Devices, Xinjiang Technical Institute of Physics and Chemistry of CAS, Urumqi 830011, China*
[3]*Department of Physics, Tamkang University, New Taipei City 25137, Taiwan*

(Received December 1, 2016; accepted February 13, 2017; published online March 28, 2017)

In order to explore new nonlinear optical (NLO) crystals with superior performance, it is greatly desirable to understand the intrinsic relationship between the microscopic structural features and macroscopic optical properties of crystals. In this paper, the electronic structures and optical properties of $Mg_3B_7O_{13}Cl$ (MBOC), which contains B_7O_{13} functional building blocks, were investigated to understand the structure — optical property relationship by first-principles calculation. Our calculated results show that the large band gap and the moderate second-harmonic generation (SHG) coefficient of MBOC (8.43 eV and $d_{32} = 0.41$ pm/V) are comparable to those of $KBe_2BO_3F_2$ (8.64 eV and $d_{11} = 0.46$ pm/V). The origin of the large band gap and the moderate SHG response of MBOC were explained by combining electronic structure analysis and the SHG density method.

1. Introduction

In recent years, nonlinear optical (NLO) materials have attracted much research interest owing to their important roles in the solid-state laser to generate ultraviolet (UV) or deep-ultraviolet (deep-UV) coherent light via frequency conversion.[1–3] From the practical viewpoint, UV or deep-UV second-harmonic generation (SHG) NLO materials with improved performance should satisfy the following criteria: a wide band gap, large SHG effect, moderate birefringence to meet the phase-matching condition, high stability, and good growth habit. Up to now, $KBe_2BO_3F_2$ (KBBF) is the only material that can generate deep-UV coherent light by direct SHG.[4] Unfortunately, the KBBF crystal is very difficult to grow with large thickness owing to its strong layered growth habit, and it contains the highly toxic BeO, which severely hinders its practical applications.[5,6] β-BaB_2O_4 (BBO) is a commercial crystal that can generate laser emission at 205 nm with frequency conversion, but its long deep-UV cutoff edge restrains its effective application in the deep-UV range.[7–9] The tetrahedral BO_4 groups existing in LiB_3O_5 (LBO),[10] CsB_3O_5,[11] and $CsLiB_6O_{10}$[12] crystals destroy the π-conjugated orbital in the planar B_3O_6 group, enlarging the band gaps of the crystals. However, the crystals with BO_4 groups as building blocks are usually characterized by small NLO coefficients. For example, the NLO coefficient d_{31} of the $Li_2B_4O_7$ crystal is 0.15 pm/V.[13]

Recently, first-principles methods have been used to calculate optical properties.[14,15] After detailed investigations of the SHG response of a series of famous borates, Lin et al., pointed out that reliable results could be obtained in comparison with experimental values.[16,17] In the search for promising NLO materials that have a large band gap and strong SHG response, the structure of $Mg_3B_7O_{13}Cl$ (MBOC), which contains B_7O_{13} functional building blocks, has captured our attention. The crystal structure of MBOC with the space group $Pca2_1$ was first obtained by Ito et al.[18] The functional building blocks, B_7O_{13}, consist of six strong distorted BO_4 groups and one BO_3 group. As shown in previous studies, the acentric strongly distorted BO_4 groups not only dominate the band gaps but also determine the SHG coefficients.[19] Curiously, does the BO_4-rich MBOC not only have a large band gap but also an unexpected SHG response comparable to that of KBBF? Up to now, due to the difficulty in synthesis and growth, detailed investigations on the optical properties of MBOC are still rare.[20–23]

In this work, we pay close attention to the band gap and SHG response of MBOC, as examined by the ab initio method based on the density functional theory. The results show that MBOC has a large band gap of 8.43 eV and a moderate SHG response of $0.9 \times$ KBBF. To clarify the mechanism behind the large band gap and SHG response, the correlation between the optical properties and structure was discussed by combining the electronic structure analysis and SHG density method.

2. Numerical Calculation Details

Geometric optimization, electronic structures, and optical properties were determined by the density functional theory (DFT) method in the CASTEP package.[24,25] The generalized gradient approximation (GGA) with the Perdew–Burke–Ernzerhof (PBE) functional was adopted.[25–27] Norm-conserving pseudopotentials[27] were used, and 770 eV was given as the plane-wave basis energy cutoff, which ensures a total energy convergence within 1.0×10^{-6} eV/atom. The Monkhorst–Pack k-point was set as $2 \times 2 \times 4$, which makes the sampling spacing finer than 0.05 A^{-1}. There are 816 empty bands (3 times the number of valence bands) involved in the calculation to ensure the convergence of SHG coefficients.

In the present work, the formula of second-order NLO susceptibility at the zero frequency limit can be derived as[28–30]

$$\chi^{(2)}_{\alpha\beta\gamma} = \chi^{(2)}_{\alpha\beta\gamma}(\mathrm{VE}) + \chi^{(2)}_{\alpha\beta\gamma}(\mathrm{VH}), \tag{1}$$

where

$$\chi^{(2)}_{\alpha\beta\gamma}(\mathrm{VH}) = \frac{e^3}{2\hbar^2 m^3} \sum_{vv'c} \int \frac{d^3k}{4\pi^3} P(\alpha\beta\gamma)\, \mathrm{Im}[p^{\alpha}_{vv'} p^{\beta}_{v'c} p^{\gamma}_{cv}]$$

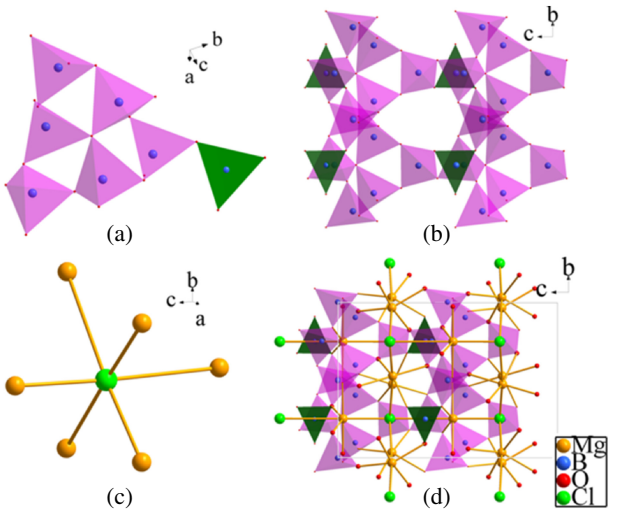

Fig. 1. (Color online) Crystal structure of MBOC: (a) B_7O_{13} group, (b) four B_7O_{13} groups, (c) ClMg6 octahedron, and (d) crystal structure of MBOC.

$$\times \left(\frac{1}{\omega_{cv}^3 \omega_{v'c}^2} + \frac{2}{\omega_{vc}^4 \omega_{cv'}} \right), \tag{2}$$

$$\chi^{(2)}_{\alpha\beta\gamma}(\mathrm{VE}) = \frac{e^3}{2\hbar^2 m^3} \sum_{vcc'} \int \frac{d^3k}{4\pi^3} P(\alpha\beta\gamma)\, \mathrm{Im}[p^{\alpha}_{vc} p^{\beta}_{cc'} p^{\gamma}_{c'v}]$$
$$\times \left(\frac{1}{\omega_{cv}^3 \omega_{vc'}^2} + \frac{2}{\omega_{vc}^4 \omega_{c'v}} \right). \tag{3}$$

Here α, β, and γ are Cartesian components, v and v' denote valence bands, c and c' denote conduction bands, and $P(\alpha\beta\gamma)$ denotes full permutation. The band energy difference and momentum matrix elements are denoted as ω_{ij} and p^{α}_{ij}, respectively. The SHG coefficient components are relevant to second-order nonlinear susceptibilities, $d_{ijk} = \chi_{ijk}/2$. Normally, d_{ijk} is abbreviated as d_{il} with the following subscript relationship between jk and l: $11 \to 1$; $22 \to 2$; $33 \to 3$; $23, 32 \to 4$; $13, 31 \to 5$; and $12, 21 \to 6$.[31)]

3. Results and Discussion

3.1 *Geometric crystal structure*

MBOC crystallizes into a crystal structure with the space group $Pca2_1$ in which the inversion is absent. The calculated equilibrium lattice parameters of a stress-free MBOC crystal are $a = 8.6559$ Å, $b = 8.6320$ Å, and $c = 12.2108$ Å, which are in good agreement with the experimental results of $a = 8.5489$ Å, $b = 8.5362$ Å, and $c = 12.0662$ Å.[23)] MBOC exhibits a three-dimensional (3D) borate framework. Six BO_4 units (B1O_4–B6O_4) and one B7O_3 unit connected by shared O atoms to form B_7O_{13} functional building blocks can be written as 7:[(1Δ + 6T)] according to Christ and Clark[32)] [Fig. 1(a)]. Four B_7O_{13} units with different stereo-isomeric configurations are further connected via bridging oxygen atoms to give a three-dimensional B–O network [Fig. 1(b)]. The B_7O_{13} groups and ClMg6 octahedron [Fig. 1(c)] are interwoven to form an intricate 3D network [Fig. 1(d)].

3.2 *Origin of large band gap*

A direct band gap of 5.56 eV is calculated for MBOC [Fig. 2(a)]. It is well known that owing to the limitation of the DFT method, local XC functionals such as GGA-PBE always underestimate the band gap. Besides GGA-PBE methods, the nonlocal (hybrid) XC functional PBE0 has also been utilized to estimate the band gaps in this work. The PBE0 functional gives a reliable estimate of the band gap energy of about 8.43 eV. By the same method described above, the calculated band gap of KBBF was obtained using the GGA functional and PBE0 functional (see Table I). The PBE0 functional gives a reliable band gap of about 8.64 eV for KBBF, which is very close to the experimentally measured value of about 8.43 eV.[4)] It should be noted that the calculated band gap of MBOC (8.43 eV) is also comparable to that of the crystal in the deep-UV region, such as KBBF (8.64 eV). Figure 2(b) shows the partial density of states (PDOS) diagrams. The top of the valence bands of MBOC is mainly derived from the O-*p* states and Cl-*p* states. The bottom of the conduction band is due to B-*sp* mixed states and Mg *s* states. Evidently, the dominant component of the band gap is B and O atoms.

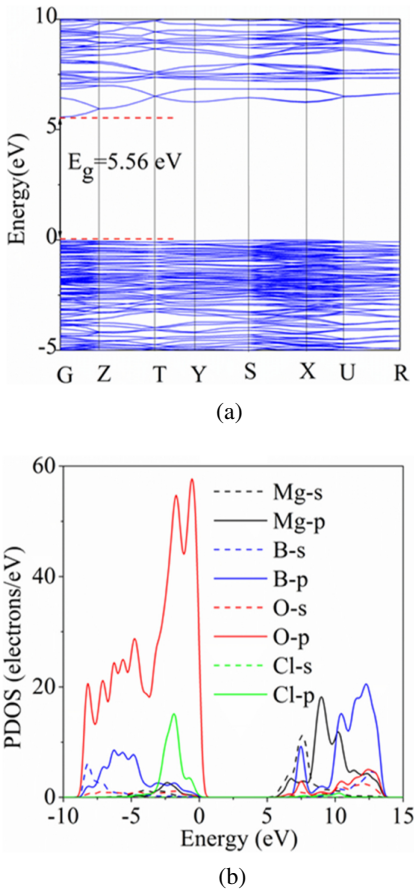

Fig. 2. (Color online) Band structures (a) and the PDOS (b) of MBOC.

Table I. Band gaps (eV) based on various exchange and correlation functionals.

Crystal	GGA	PBE0	Experiment
MBOC	5.56	8.43	—
KBBF	6.08	8.64	8.43[4)]

According to the frontier molecular orbitals theory, the band gaps ΔE_g of the different borate anionic groups obey the following relative orders: $\Delta E_g(BO_4) > \Delta E_g(BO_3) \approx \Delta E_g(B_3O_7) > \Delta E_g(B_3O_6)$.[14)] According to Chen et al.

Table II. SHG coefficients (pm/V) of MBOC and KBBF with a correction of the band gap using scissors operators.

Crystal	Calculated SHG coefficients (pm/V)
MBOC	$d_{31} = -0.31$; $d_{32} = 0.41$; $d_{33} = 0.08$
KBBF	$d_{11} = 0.47$

results, introducing BO_4 groups to the structures can enlarge the band gaps.[14] For example, the β-BaB_2O_4 crystal, in which the basic unit is the B_3O_6 group, displays a deep-UV cutoff edge at 185 nm;[9] LiB_3O_5 with the basic B_3O_7 units of two BO_3 and one BO_4, has a short cutoff edge at 155 nm;[10] SrB_4O_7 exclusively containing BO_4 groups has a lower cutoff edge (down to 130 nm) than KBBF (147 nm) exclusively containing BO_3 groups.[4,33] From the viewpoint of the structure of MBOC with B_7O_{13} groups, MBOC has a large band gap similar to that of LiB_3O_5 (8 eV).[10]

3.3 *Origin of strong SHG response*

Using Eq. (1), the SHG coefficients of MBOC are calculated with band structures. The scissors operator of MBOC (2.87 eV) and that of KBBF (2.56 eV) are used to compensate the underestimation in the band structure calculations of the optical properties. The MBOC belongs to the *mm*2 point group, and owing to symmetry restriction,[34] there are only three independent elements: $d_{15} = d_{31}$, $d_{24} = d_{32}$, and d_{33} (see Table II). To identify the contribution of each atom in the SHG processes in real space, a SHG density technique is adopted. It was performed by using the effective SHG of each band (occupied and unoccupied) as a weighting coefficient [after normalization with the total virtual electron (VE) or virtual hole (VH) $\chi^{(2)}$] to sum the probability densities of all occupied or unoccupied states. The effective SHG of each band can be obtained by a so-called "band resolved $\chi^{(2)}$ analysis" scheme, which means that by fixing one of the three band indices of formulas (2) or (3) and summing the other band indices, one can obtain the effective SHG due to that given index.[35] The SHG density method can hence ensure that the quantum states irrelevant to SHG will not be shown in these occupied or unoccupied "SHG densities", and the resulting distribution of such density represents a highlight of the origin of SHG optical nonlinearity in real space.[36] The VE contributions to the coefficients of MBOC are 91.5% (d_{31}), 96.7% (d_{32}), and 97.2% (d_{33}). In order to identify the contributions from different structural groups to the SHG effect, here we show the SHG density for the VE process of the largest SHG tensors d_{32} (see Fig. 3). It is clear that the oxygen atoms give the dominant contribution to the SHG coefficients for both virtual-electron-occupied states and unoccupied states. The B4, B5, and B7 atoms play an important role in the virtual-electron contribution for unoccupied states. It is clear that the trilateral BO_3 groups and the tetrahedral BO_4 groups cooperate to dominate the contribution to the SHG response.

It is noted that the SHG coefficient $d_{32} = 0.41$ pm/V of MBOC is comparable to that of KBBF ($d_{11} = 0.46$ pm/V) and is consistent with the experimental value of 0.47 pm/V. The unexpected SHG response of MBOC is a result of abundant of BO_4. Why does MBOC exhibit a moderate SHG response of 0.9 × KBBF? We first applied the anionic group concept,[37] which suggests that macroscopic SHG behavior mainly originates from the geometrical superposition of the microscopic second-order susceptibility of the NLO-active anionic groups. The B1–B6 atoms are tetrahedrally coordinated to oxygen atoms, generating the $B1O_4$–$B6O_4$ tetrahedral with B–O bond lengths varying from 1.448(3) to 1.572(4) Å. The B7 atoms are triangularly coordinated to oxygen atoms with B–O bond lengths varying from 1.373(1) to 1.377(1). The magnitude of the distortion was further calculated using $\Delta d = |\sum_i \boldsymbol{r}_i|$, in which $\boldsymbol{r}_i$ is the displacement vector of the ith B–O bond.[38] For ideal BO_x ($x = 3, 4$) groups, the magnitude of Δd should be zero. The obtained Δd of BO_x ($x = 3, 4$) groups in MBOC is shown in Table III. It is clear that the BO_x ($x = 3, 4$) groups are strongly distorted, especially $B4O_4$, $B5O_4$, and $B7O_3$. We also calculated the Δd of BO_x ($x = 3, 4$) groups of LBO containing BO_3 and BO_4 groups for comparison (Table III). Evidently, the Δd values of BO_x ($x = 3, 4$) in LBO are also large, corresponding to a large SHG response (3 × KDP). As shown in a previous experimental observation, the BO_4 groups with the large distortions give dominant contributions to the SHG response, such as in $Cs_2B_4SiO_9$.[39] Therefore, the strongly distorted BO_x ($x = 3, 4$) groups of MBOC may result in an unexpected SHG response.

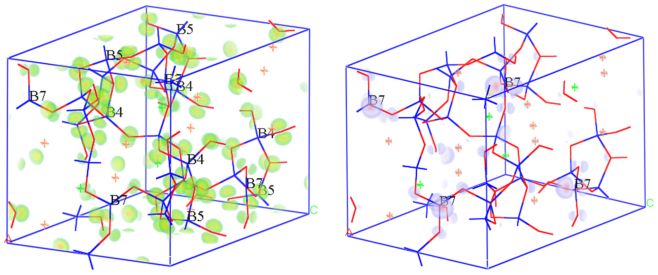

(a) (b)

Fig. 3. (Color online) SHG density of the VE of the largest SHG tensors of MBOC: (a) occupied states; (b) unoccupied states.

Table III. Magnitude of distortion Δd of BO_x ($x = 3, 4$) groups in MBOC and LBO.

Compounds	Groups	Δd
MBOC	$B1O_4$	0.106
	$B2O_4$	0.071
	$B3O_4$	0.107
	$B4O_4$	0.180
	$B5O_4$	0.182
	$B6O_4$	0.146
	$B7O_3$	0.241
LBO	$B1O_4$	0.224
	$B2O_3$	0.151
	$B3O_3$	0.183

4. Conclusions

We have systematically investigated the electronic and optical properties of MBOC using first-principles calculations. The calculation results show that MBOC has a large calculated band gap of 8.43 eV, which is comparable to that of KBBF (8.64 eV), resulting from the introduction of the BO_4 groups to the structure of MBOC. The unexpected SHG

response of MBOC of about 0.9 × KBBF may originate from the strongly distorted BO_x ($x = 3, 4$) groups. This result indicates that MBOC may be a promising NLO material in the UV or even the deep-UV region. One may be able to design new NLO compounds with large band gaps and moderate SHG responses by inserting B_7O_{13} functional building blocks consisting of strongly distorted BO_x ($x = 3, 4$) groups.

Acknowledgements

This work was supported by the National Key Basic Research Program of China (Grant No. 2014CB648400), Xinjiang High-level Talent Project and MOST 104-2112-M-032-001, the National Natural Science Foundation of China (Grant Nos. 11164027, 51425206, and 11474353), and the Xinjiang International Science & Technology Cooperation Program (20146001).

*zhyang@ms.xjb.ac.cn

1) K. Xu, P. Loiseau, and G. Aka, J. Cryst. Growth **311**, 2508 (2009).
2) P. S. Halasyamani and K. R. Poeppelmeier, Chem. Mater. **10**, 2753 (1998).
3) K. M. Ok, E. O. Chi, and P. S. Halasyamani, Chem. Soc. Rev. **35**, 710 (2006).
4) C. T. Chen, G. L. Wang, X. Y. Wang, and Z. Y. Xu, Appl. Phys. B **97**, 9 (2009); Y. N. Xia, C. T. Chen, D. Y. Tang, and B. C. Wu, Adv. Mater. **7**, 79 (1995).
5) P. Yu, L. M. Wu, L. J. Zhou, and L. Chen, J. Am. Chem. Soc. **136**, 480 (2014).
6) S. Zhao, P. Gong, L. Bai, X. Xu, S. Zhang, Z. Sun, Z. Lin, M. Hong, C. Chen, and J. Luo, Nat. Commun. **5**, 4019 (2014).
7) J. Lin, M. H. Lee, Z. P. Liu, C. T. Chen, and C. J. Pickard, Phys. Rev. B **60**, 13380 (1999).
8) V. G. Dmitriev, G. G. Gurzadyan, and D. N. Nikogosyan, *Handbook of Nonlinear Optical Crystals* (Springer, Berlin, 1999) p. 67.
9) J. Li, Z. J. Ma, C. He, Q. H. Li, and K. C. Wu, J. Mater. Chem. C **4**, 1926 (2016).
10) C. T. Chen, Y. C. Wu, A. D. Jiang, B. C. Wu, G. M. You, R. K. Li, and S. J. Lin, J. Opt. Soc. Am. B **6**, 616 (1989).
11) Y. C. Wu, T. Sasaki, S. Nakai, A. Yokotani, H. G. Tang, and C. T. Chen, Appl. Phys. Lett. **62**, 2614 (1993).
12) Y. Mori, I. Kuroda, S. Nakajima, T. Sasaki, and S. Nakai, Appl. Phys. Lett. **67**, 1818 (1995).
13) T. Sugawara, R. Komatsu, and S. Uda, Solid State Commun. **107**, 233 (1998).
14) C. T. Chen, Z. S. Lin, and Z. Wang, Appl. Phys. B **80**, 1 (2005).
15) F. Qin and R. K. Li, J. Cryst. Growth **318**, 642 (2011).
16) Z. S. Lin, L. Kang, T. Zheng, R. He, H. Huang, and C. T. Chen, Comput. Mater. Sci. **60**, 99 (2012).
17) Z. S. Lin, X. X. Jiang, L. Kang, P. F. Gong, S. Y. Luo, and M.-H. Lee, J. Phys. D **47**, 253001 (2014).
18) T. Ito, N. Morimoto, and R. Sadanaga, Acta Crystallogr. **4**, 310 (1951).
19) P. Becker, Adv. Mater. **10**, 979 (1998).
20) E. Dowty and J. R. Clark, Solid State Commun. **10**, 543 (1972).
21) E. Dowty and J. R. Clark, Z. Kristallogr. **138**, 64 (1973).
22) M. B. Zagudailova, P. A. Plachinda, P. S. Berdonosov, S. Yu. Stefanovich, and V. A. Dolgikh, Inorg. Mater. **41**, 393 (2005).
23) X. B. Qiao and H. J. Seo, J. Am. Ceram. Soc. **98**, 594 (2015).
24) S. J. Clark, M. D. Segall, C. J. Pickard, P. J. Hasnip, M. I. J. Probert, K. Refson, and M. C. Payne, Z. Kristallogr. **220**, 567 (2005).
25) B. G. Pfrommer, M. Cote, S. G. Louie, and M. L. Cohen, J. Comput. Phys. **131**, 233 (1997).
26) J. P. Perdew, K. Burke, and M. Ernzerhof, Phys. Rev. Lett. **77**, 3865 (1996).
27) A. M. Rappe, K. M. Rabe, E. Kaxiras, and J. D. Joannopoulos, Phys. Rev. B **41**, 1227 (1990).
28) C. Aversa and J. E. Sipe, Phys. Rev. B **52**, 14636 (1995).
29) J. S. Lin, A. Qteish, M. C. Payne, and V. Heine, Phys. Rev. B **47**, 4174 (1993).
30) B. Zhang, M.-H. Lee, Z. Yang, Q. Jing, S. Pan, M. Zhang, H. Wu, X. Su, and C.-S. Li, Appl. Phys. Lett. **106**, 031906 (2015).
31) R. W. Boyd, *Nonlinear Optics* (Academic, New York, 2008) p. 39.
32) C. L. Christ and J. R. Clark, Phys. Chem. Miner. **2**, 59 (1977).
33) A. I. Zaitsev, A. S. Aleksandrovskii, A. V. Zamkov, and A. M. Sysoev, Inorg. Mater. **42**, 1360 (2006).
34) D. A. Kleinman, Phys. Rev. **126**, 1977 (1962).
35) M.-H. Lee, C.-H. Yang, and J.-H. Jan, Phys. Rev. B **70**, 235110 (2004).
36) C.-H. Lo, Dr. thesis, Department of Physics, Tamkang University, Taiwan (2005).
37) C. T. Chen, Y. C. Wu, and R. K. Li, Int. Rev. Phys. Chem. **8**, 65 (1989).
38) Q. Jing, Z. Yang, S. Pan, and D. Xue, Phys. Chem. Chem. Phys. **17**, 21968 (2015).
39) H. P. Wu, H. W. Yu, S. L. Pan, Z. J. Huang, Z. H. Yang, X. Su, and K. R. Poeppelmeier, Angew. Chem., Int. Ed. **52**, 3406 (2013).